

ON THE UNIVERSAL GEV EMISSION IN BINARY-DRIVEN HYPERNOVAE AND THEIR INFERRED MORPHOLOGICAL STRUCTURE

R. RUFFINI^{1,2,3,4}, R. MORADI^{1,3}, Y. WANG^{1,3}, Y. AIMURATOV^{1,2,5}, M. AMIRI^{3,6}, L. BECERRA^{1,3}, C. L. BIANCO^{1,3}, Y.-C. CHEN^{1,3}, B. ESLAM PANAH^{3,7}, G. J. MATHEWS⁸, M. MUCCINO⁹, G. B. PISANI^{1,3}, D. PRIMORAC^{1,3}, J. A. RUEDA^{1,3,4}

Draft version June 14, 2022

ABSTRACT

We address the significance of the observed GeV emission from *Fermi*-LAT on the understanding of the structure of long GRBs. We examine 82 X-ray Flashes (XRFs), in none of them GeV radiation is observed, adding evidence to the absence of a black hole (BH) formation in their merging process. By examining 329 Binary-driven Hypernovae (BdHNe) we find that out of 48 BdHNe observable by *Fermi*-LAT in *only* 21 of them the GeV emission is observed. The GeV emission in BdHNe follows a universal power-law relation between the luminosity and time, when measured in the rest frame of the source. The power-law index in BdHNe is of -1.20 ± 0.04 , very similar to the one discovered in S-GRBs, -1.29 ± 0.06 . The GeV emission originates from the newly-born BH and allows to determine its mass and spin. We further give the first evidence for observing a new GRB subclass originating from the merging of a hypernova (HN) and an already formed BH binary companion. We conclude that the GeV emission is a necessary and sufficient condition to confirm the presence of a BH in the hypercritical accretion process occurring in a HN. The remaining 27 BdHNe, recently identified as sources of flaring in X-rays and soft gamma-rays, have no GeV emission. From this and previous works, we infer that the observability of the GeV emission in some BdHNe is hampered by the presence of the HN ejecta. We conclude that the GeV emission can only be detected when emitted within a half-opening angle $\approx 60^\circ$ normal to the orbital plane of the BdHN.

Keywords: gamma-ray bursts: general — binaries: general — stars: neutron — supernovae: general — black hole physics — hydrodynamics

1. INTRODUCTION

The supernovae (SNe) associated with long gamma-ray bursts (long-GRBs) are peculiar in three aspects: a) they are type Ic SNe, missing hydrogen (H) and helium (He) emission lines, b) they have very broad-line spectra implying unusually high expansion velocity all the way to $0.2 c$, and c) they are systematically more energetic, at least by a factor 10^2 , than the typical SNe Ic (see e.g. Woosley & Bloom 2006; Della Valle 2011; Hjorth & Bloom 2012). The name *hypernova* (HN) was introduced to designate these phenomena. On the ground of these observations, it has been suggested that such HNe are likely occurring in binary systems (Smartt 2009). Processes of energy injection have been also invoked to justify their outstanding energetics (Lyman et al. 2016).

In parallel to this sequence of observational discoveries, the theories of long GRBs have also made a sig-

nificant progress. The traditional model of all long-GRBs, assumed to occur on an ultra-relativistic jetted emission originating from a black hole (BH) (see e.g. Woosley 1993; Paczyński 1998; MacFadyen & Woosley 1999; Bromberg et al. 2013), has been superseded by recognizing the existence of three subclasses of long-GRBs, all with binary progenitors: 1) the X-ray flashes (XRFs), 2) the binary-driven hypernovae (BdHNe), and 3) the BH-HN binary. They share a common progenitor namely a CO_{core} in a tight binary system with a neutron star (NS) or a BH. The CO_{core} undergoes a SN explosion with the creation of a new NS (νNS). If the hypercritical accretion of the SN ejecta onto the NS companion is not sufficient to reach the NS critical mass, then the XRF occurs. When a BH is already present or formed in the hypercritical accretion onto the NS, a BdHN occurs. A νNS -NS binary is the final state (*out-state*) of XRF with an X-ray emission of isotropic energy $\lesssim 10^{52}$ erg and spectrum with a peak value $E_{p,i} \lesssim 0.3$ MeV. In BdHN the out-state is a binary νNS -BH system with an X-ray emission of isotropic energy $\gtrsim 10^{52}$ erg and spectrum with the peak $E_{p,i} \gtrsim 0.2$ MeV.

These novel results have been recently summarized in three extended articles (Ruffini et al. 2016b; Becerra et al. 2016; Ruffini et al. 2018a) based on works developed in preceding years and full references are there given. The fundamental role of neutrinos has been also recently discussed in Becerra et al. (2018b).

The aim of this article is to use the GeV emission of *Fermi*-LAT for further differentiating the seven different families of GRBs presented in Ruffini et al. (2016b), in particular we here sanction the difference between XRFs

¹ ICRA and Dipartimento di Fisica, Università di Roma “La Sapienza”, Piazzale Aldo Moro 5, I-00185 Roma, Italy

² Université de Nice Sophia-Antipolis, Grand Château Parc Valrose, Nice, CEDEX 2, France

³ International Center for Relativistic Astrophysics Network, Piazza della Repubblica 10, I-65122 Pescara, Italy

⁴ ICRANet-Rio, Centro Brasileiro de Pesquisas Físicas, Rua Dr. Xavier Sigaud 150, 22290-180 Rio de Janeiro, Brazil

⁵ Fesenkov Astrophysical Institute, Observatory 23, 050020 Almaty, Kazakhstan

⁶ Department of Physics, Isfahan University of Technology, 84156-83111, Iran

⁷ Physics Department and Biruni Observatory, College of Sciences, Shiraz University, Shiraz 71454, Iran

⁸ Center for Astrophysics, Department of Physics, University of Notre Dame, Notre Dame, IN, 46556, USA

⁹ Istituto Nazionale di Fisica Nucleare, Laboratori Nazionali di Frascati, I-00044 Frascati, Italy

and BdHNe.

By analyzing of all XRFs with known redshift we confirm that in none of them GeV radiation has been observed. This further confirms the conclusion, previously reached solely on the ground of the energetics and spectral properties of XRFs, that in this case no BH is formed in the hypercritical accretion of the HN into the NS companion (Ruffini et al. 2016b), which firmly characterizes their difference from BdHNe.

Turning to the BdHNe we focus attention on 48 sources with unambiguous quality of the data restricting to sources which are, at trigger time, within the boresight angle of the *Fermi*-LAT. We identify two BdHNe subclasses, 21 emitting GeV radiation and the remaining 27 ones with X-ray and Gamma-ray flaring activities and not emitting GeV radiation. To the ones emitting the GeV radiation we initially apply the same approach already successfully adopted in the case of S-GRBs (see Ruffini et al. 2018b) evidencing the existence of a universal behavior of the power-law relation between the 0.1–100 GeV luminosity light-curve versus time in the rest frame of the GRBs, $L_n = A_n t^{-1.20 \pm 0.04} \text{ erg s}^{-1}$. While in S-GRBs the amplitude, A_n , is universal, in the case of BdHNe the amplitude is strongly dependent on the total energy of the source. Their power law slope of -1.20 ± 0.04 is, instead, universal and very similar to the one discovered in S-GRBs, -1.29 ± 0.06 .

Following the same procedure in the S-GRBs 1) we estimate the mass and spin of the BH, 2) we further present the correlation of luminosity and GeV energy with the E_{iso} of the source and 3) we evidence the existence, in the most energetic ones, of accretion onto an already formed BH.

We conclude in total generality that the GeV emission also in BdHNe indicates the necessary and sufficient condition for the existence of the BH in the accretion process of the HN ejecta either on a NS or an already formed BH.

For the first time, evidenced by the presence or absence of GeV emission in BdHNe, we present in this article a novel toroidal morphology of the HN accretion, see section 7. This conclusion has been reached by exploiting three main results: 1) the evidence for the existence of BdHNe with GeV emission in 21 sources and the existence of an almost equal number without the GeV emission, namely 27 sources; 2) the consequent inference based on the above numerical evidence of the existence of a toroidal geometry in the hypercritical accretion process of the HN ejecta (see section 7); 3) the visualization of these results using numerical analysis presented in Berra et al. (2016, 2018a).

We first give in section 2 an outline of the seven GRB subclasses presented in Ruffini et al. (2016b) with a brief summary of their initial states (*in-state*), their out-state, and their energetics and spectral properties both in the gamma-rays and in the GeV emission.

In section 3 a summary of observational properties of 48 XRFs observed after the launch of *Fermi*, including their cosmological redshifts, $E_{p,i}$ of their spectrum, their isotropic energy E_{iso} , the Fermi GCN and the boresight angle of *Fermi*-LAT (if observed) are given. As predicted, in none of them GeV emission is observed.

In order to test the properties of the GeV emission in BdHNe, we consider only the ones which have the boresight angle of *Fermi*-LAT less than 75° at the time

of the trigger. We give the details of the 48 BdHNe, out of the 329 BdHNe with known cosmological redshifts (Pisani et al. 2016). We enumerate the members of the two subclasses of BdHNe: 21 with GeV emission and 27 BdHNe without GeV emission.

In section 4 the observational properties of 21 BdHNe with observed GeV emission are presented. For each BdHN of this group the cosmological redshift, the $E_{p,i}$ of the spectrum, the E_{iso} of the source, the Fermi GCN, the boresight angle, the E_{LAT} , the likelihood test statistic (TS) and some distinguishing properties are given in Table 4. For each of the these 21 BdHNe the 0.1–100 GeV luminosity light-curves as a function of time in the rest-frame of the source is given. We report for each source the value of amplitude A_n with the associated uncertainty, the power-law index α , and the luminosity at 10 s from the beginning of the prompt radiation with their uncertainties. We also provide the correlation between luminosity at 10 s and E_{iso} .

In section 5 in correspondence of each BdHN we determine, following the approach already adopted in accompanying paper (Ruffini et al. 2018b) for the case of S-GRBs, the BH mass and the spin. For each BdHN we tabulate the value of the mass and spin of the BH adopting two indicative NS relativistic equation of states (EOS). We show that the birth of a BH in an hypercritical accretion process of an HN is a necessary and sufficient condition to explain the GeV emission.

In section 6 we address the new family of the long GRBs, the subclass of BH-HN, originating in a binary progenitor composed of a CO_{core} and associated binary BH, we give 5 examples of these systems which are by far the most energetic subset of BdHNe.

In section 7 the cosmological redshift, the $E_{p,i}$ of the spectrum, the E_{iso} of the source, the Fermi GCN, the boresight angle and some distinguishing properties of 27 BdHNe without GeV emission are given. We explain the nature of the these BdHNe in terms of a novel morphology of the binary system. The unexpected result appeared that the geometry of BdHNe, in some respect, is similar to the one of Active Galactic Nuclei (AGN). In the case of BdHNe the GeV emission is constrained by the HN ejecta to be observable only through conical region normal to the orbital binary plane. When the BdHNe are seen along the orbital plane of the binary progenitor then the GeV emission is scattered by the HN ejecta and only the Gamma-ray flare, the X-ray flare and the X-ray plateau remain observable. When the GRB is observed in a conical region of approximately 60° around the normal to the plane of the binary progenitors, then all the emissions are observable, namely the X-ray, the gamma-ray and also the GeV emission.

In section 8 we visualize this novel geometry using the result of recent smoothed-particle-hydrodynamics (SPH) numerical simulations at the moment of BH formation in a BdHN and finally we proceed to the general conclusions.

Before proceeding we indicate in Table 1 the alphabetic ordered list of acronyms used in this work.

2. SUMMARY OF THE SEVEN SUBCLASSES OF GRBS

In this paper we address the specific role of the GeV radiation in order to further characterize the seven subclass of GRBs presented in Ruffini et al. (2016b); in

Extended wording	Acronym
Binary-driven hypernova	BdHN
Black hole	BH
Carbon-oxygen core	CO _{core}
Gamma-ray burst	GRB
Gamma-ray flash	GRF
Massive neutron star	M-NS
Neutron star	NS
New neutron star	ν NS
Short gamma-ray burst	S-GRB
Short gamma-ray flash	S-GRF
Supernova	SN
Ultrashort gamma-ray burst	U-GRB
White dwarf	WD
X-ray flash	XRF

Table 1

Alphabetic ordered list of the acronyms used in this work.

particular we characterize the difference between XRFs and BdHNe. For this goal we will just considered in the following sources after the launch of *Fermi* when LAT data became available. We have therefore correspondingly updated the number presented in Fig. 38 in Ruffini et al. (2018a). In Table 2 we have indicated, for each GRB subclass, their name, the number of observed sources with definite cosmological redshift, their progenitors characterizing their “in-state”: in all cases the progenitors are binary systems composed of various combinations of CO_{core}, undergoing a SN explosion, of the ν NS created in such SN explosion, of NS, of white dwarfs (WDs), of a BH. The “out-state” of the merging process, have been represented in Fig. 7 in Ruffini et al. (2016b).

The case of the S-GRF and S-GRB has been the subject of the accompanying paper (Ruffini et al. 2018b). We have shown there the special role of the GeV radiation in differentiating the S-GRF without GeV emission and the S-GRBs *always* presenting the GeV radiation. These results imply a substantial symmetry in the emission process and the absence of the jetted emission. The existence of the universal relation of the 0.1–100 GeV luminosity as a function of time when measured in the rest frame of the source of S-GRBs was there described: the specific power-law identified with normalization of 0.88 ± 0.13 and slope index of -1.29 ± 0.06 . In that paper we inferred a minimum BH mass in the range of $2.24\text{--}2.89M_{\odot}$ and a corresponding maximum dimensionless spin in the range of 0.18–0.33, showing their role in identifying the energy sources of the GeV radiation.

We here turn to the case of long GRBs. Two possible progenitor systems of long GRBs have been identified (Ruffini et al. 2016b): a binary system composed of a CO_{core}, exploding as SN Ic, and a NS companion (see, e.g., Ruffini et al. 2001c; Rueda & Ruffini 2012; Fryer et al. 2014); and an analogous binary system where the binary companion of the exploding CO_{core} is an already formed BH. Binary X-ray sources such as Cygnus-X1 are possible progenitors of such systems. We address first the system with the NS binary companion and then give the first evidence of five alternative systems with a BH companion, in the most energetic GRB sources.

As the SN ejecta from the exploding CO_{core} engulfs the close NS binary companion (Becerra et al. 2015, 2016) a hypercritical accretion process occurs with the emission

of $\nu\bar{\nu}$ pairs and, for tight binaries, the formation of an e^+e^- plasma (Rueda & Ruffini 2012). The presence of a NS companion explains the observed removing the outer layers of the CO_{core} (Fryer et al. 2014).

Also in long bursts a differentiation into two subclasses exists (see, e.g., Ruffini et al. 2015a, 2016b). When the orbital period of the binary system is $\gtrsim 5$ min, the hypercritical accretion is not sufficient to trigger the collapse of the NS companion into a BH. Therefore, a MNS is formed creating a binary with the ν NS originated in the SN explosion of the CO_{core}. An associated X-ray flash (XRF) with $E_{\text{iso}} < 10^{52}$ erg and $E_{\text{p},i} < 0.3$ MeV is in this case emitted (Ruffini et al. 2015a; Becerra et al. 2015, 2016; Ruffini et al. 2016b). In particular 48 sources for XRFs have been indicated with their “in-states” represented by a CO_{core}-NS binary and their “out-state” represented by a ν NS, originated in the SN explosion of a CO_{core} and a NS companion. Their spectral peak energy is in the range $4 \text{ keV} < E_{\text{p},i} < 300 \text{ keV}$ isotropic energy $10^{48} \lesssim E_{\text{iso}} \lesssim 10^{52}$ erg. No GeV emission has been observed in these sources. The complete list of XRFs which updates the one in Ruffini et al. (2016b) is given in section 7.

When the orbital period is as short as ≈ 5 minutes, the hypercritical accretion proceeds at higher rates and the companion NS reaches its critical mass leading to 1) the formation of a BH in a binary system with the ν NS (Fryer et al. 2015), 2) the emission of a GRB with $E_{\text{iso}} \gtrsim 10^{52}$ erg and $E_{\text{p},i} \gtrsim 0.2$ MeV, and 3) the onset of the GeV emission observed from the newly-born BH. These systems have been indicated as BdHNe (Ruffini et al. 2015a; Becerra et al. 2015; Fryer et al. 2015; Becerra et al. 2016; Ruffini et al. 2016b). The BH formation and the associated GRB emission occur seconds after the onset of the SN explosion (see, e.g., the case of GRB 090618 in Izzo et al. 2012).

The first list of BdHNe was introduced in Pisani et al. (2016); Ruffini et al. (2016b) which was further extended in Ruffini et al. (2018a) and here it is still further extended in section 4 and section 7. 329 sources have been identified after the launch of *Fermi* all with the given redshift, with their in-states represented by a CO_{core}-NS binary and their out-state represented by a ν NS, originated in the SN explosion of a CO_{core} and a companion BH, their spectral peak energy has the range $0.2 \text{ MeV} < E_{\text{p},i} < 2 \text{ MeV}$, isotropic energy $10^{52} < E_{\text{iso}} < 10^{54}$ erg and their isotropic GeV emission is $\sim 10^{52}$ erg. As explained in section 4 and section 7 two subclasses of BdHNe have been found corresponding respectively to the presence or absence of their GeV emission.

The most important new result obtained on the structure of the BdHNe has followed from the observation of the GeV emission. We have considered only the ones which have the boresight angle of Fermi LAT less than 75° at trigger time, they appear in two subclasses of BdHNe: 21 with GeV emission and 27 BdHNe without GeV emission. All their properties are given in section 4 and section 7. This result has been at first very surprising since BdHNe appear to differ from short GRBs in respect to the GeV emission, always present in S-GRBs and present in a subset of BdHNe as we show in section 7 this will leave in the totally new results on the morphology of the BDHN.

	Sub-class	Number	<i>In-state</i>	<i>Out-state</i>	$E_{p,i}$ (MeV)	E_{iso} (erg)	$E_{iso,GeV}$ (erg)
I	S-GRFs	18	NS-NS	MNS	$\sim 0.2-2$	$\sim 10^{49}-10^{52}$	–
II	S-GRBs	6	NS-NS	BH	$\sim 2-8$	$\sim 10^{52}-10^{53}$	$\gtrsim 10^{52}$
III	XRFs	49	CO _{core} -NS	ν NS-NS	$\sim 0.004-0.3$	$\sim 10^{48}-10^{52}$	–
IV	BdHNe	329	CO _{core} -NS	ν NS-BH	$\sim 0.2-2$	$\sim 10^{52}-10^{54}$	$\gtrsim 10^{52}$
V	BH-HN	5	CO _{core} -BH	ν NS-BH	$\gtrsim 2$	$> 10^{54}$	$\gtrsim 10^{53}$
VI	U-GRBs	0	ν NS-BH	BH	$\gtrsim 2$	$> 10^{52}$	–
VII	GRFs	1	NS-WD	MNS	$\sim 0.2-2$	$\sim 10^{51}-10^{52}$	–

Table 2

Summary of the GRB subclasses. In addition to the subclass name, we report the number of GRBs for each subclass updated by the end of 2016. We recall as well the “in-state” representing the progenitors and the “out-state” as well as the $E_{p,i}$ and E_{iso} for each subclass. We finally indicate the GeV emission in the last column which for the long GRBs is only for the BdHNe and BH-HN and in the case of short bursts is only for S-GRBs and in all of them the GeV emission has energy more than 10^{52} erg.

Concerning the BH-HN they are a subset of BdHNe corresponding to particularly energetic sources and BH of larger mass all the way up to $29 M_{\odot}$. Their progenitor is a CO_{core}-BH binary and their out-state represented by a ν NS, originated in the SN explosion of a CO_{core} and a companion BH. Their spectral peak energy is larger than 2 MeV, isotropic energy, $E_{iso} > 10^{54}$ erg and their isotropic GeV emission is $\sim 10^{53}$ erg.

While S-GRFs S-GRBs, XRFs and BdHNe have a significant number of sources and their statistical properties can be inferred from the GeV emission of *Fermi*-LAT, the observed number of the U-GRBs and GRFs by *Fermi* does not afford yet to derive conclusive statistical results.

3. X-RAY FLASHES (XRFs)

In our classification we have considered the case of XRFs, long GRBs associated with SNe with $E_{iso} < 10^{52}$ erg and $E_{p,i} < 300$ keV. Out of the 82 XRFs (Ruffini et al. 2018a), 48 of them are sources after the *Fermi* era and only 7 were observed by *Fermi*: 3 outside the boresight angle and 4 inside. We have seen that in none of them GeV emission has been observed and all of them have $E_{p,i} < 300$ keV and $E_{iso} < 10^{52}$ erg, see Table 3. This information confirms that all these sources originate from a progenitor of the binary CO_{core}-NS in which due to long binary separation (typically more than 10^{11} cm) the critical mass of NS is not reached and the BH is not formed. Therefore there is no GeV emission and this is consistent with the formation of a MNS and not a BH.

4. BINARY-DRIVEN HYPERNOVAE (BDHNE)

In this section, we work on the subclass of BdHN, which observationally is defined as the long GRB with $E_{iso} > 10^{52}$ erg. There are 329 BdHNe with known redshift (Ruffini et al. 2018a), out of them, we are interested only in the 48 BdHNe which have the boresight angle of *Fermi*-LAT less than 75° at the time of the trigger. Within these 48 BdHNe, nearly half of them, namely 21 BdHNe have TS value > 25 , which means to exclude at $5-\sigma$ the GeV photons from background sources. Details are shown in Table 4. Following the *Fermi* catalog (Ackermann et al. 2013) for time-resolved likelihood spectral analysis we divide the data into logarithmically spaced bins. If the TS value of each bin is smaller than 16 we merge the time bin with the next one and we repeat the likelihood analysis.

Theoretically, we expect the GeV emission occurring in BdHN, since the creation of GeV photon requires ultra-relativistic e^+e^- outflow, which can only be generated in a Kerr BH (Ruffini et al. 1999).

In the BdHN model, the BH is formed from a NS accreting part of the SN ejecta. The total mass for the SN ejecta associated with GRBs is almost standard ($M_{ej} \sim 6M_{\odot}$), therefore, the final mass of the BHs are also similar, usually a little above the NS critical mass, as it is verified in the next section. The GeV photons coming from a same mechanism, originated from similar BHs shall behave similarly, in fact, the observed light-curves of GeV emission exhibit some similarities, for instance, there is a time-delay of the first GeV photon with respect to the starting time of the gamma-ray emission, and the decaying slope of the light-curves later than the drastic early prompt phase are almost common within the uncertainties (see, e.g., Nava et al. 2014; Ruffini et al. 2015a,b, 2016a,b; Aimuratov et al. 2017, and Fig. 1). In the following, we are going to fit simultaneously the light-curves of all the 21 BdHNe with GeV emission, by assuming a same power-law decay index but different amplitudes, this assumption is consistent with our model, moreover, it brings the benefit for those GRBs with limited data that cannot be fitted solely.

We limit our analysis of the light-curves at time later than the BdHN prompt emission, when the GeV luminosity is already in the asymptotic power-law regime. A power-law

$$L_n(t) = A_n t^{\alpha} \quad (1)$$

describing the rest-frame 0.1–100 GeV isotropic luminosity light-curve of n th BdHN is assumed. In the simultaneous fitting, we perform the Levenberg-Marquardt method to perform the minimization (Gill & Wright 1981). The basic idea of fitting is to minimize the χ^2 ; when fitting one curve to one equation, the χ^2 is minimized. To fit N curves to N equations simultaneously, the sum of the χ^2 values should to be minimized. The related equations are:

$$\chi^2 = \sum_{n=1}^N \chi_n^2 \quad (2)$$

$$\chi_n^2 = \sum_{i=1}^M \frac{1}{\sigma_{ni}^2} (L_{ni} - L_n(t_{ni}, A_n, \alpha))^2 \quad (3)$$

where n represents each BdHN, i represents each data point in a given BdHN, A_n is the amplitude of a power-law function for the n th BdHN, α is the common power-law index shared for all the BdHNe. Thus, for the n th BdHN, at time t_{ni} , the observed luminosity is L_{ni} , and the predicted luminosity is $L_n(t_{ni}, A_n, \alpha)$. The value of

Group	XRF	z	E_{iso} (10^{50} erg)	XRF	z	E_{iso} (10^{50} erg)
No <i>Fermi</i> Observation	081007	0.5295	17 ± 2	120224A	1.1	37.2 ± 7.6
	090407	1.4485	50 ± 17	120422A	0.283	2.4 ± 0.8
	090417B	0.345	30.9 ± 2.7	120714B	0.3984	8.0 ± 2.0
	090814	0.696	23.6 ± 4.6	120722A	0.9586	47.0 ± 3.6
	091018	0.971	81 ± 10	120724A	1.48	58 ± 13
	100316B	1.18	11.8 ± 0.9	130511A	1.3033	16.7 ± 5.3
	100316D	0.059	0.59 ± 0.05	130604A	1.06	78 ± 15
	100418	0.624	5.21 ± 0.51	130702A	0.145	6.5 ± 1.0
	100508A	0.5201	8.7 ± 1.4	130831A	0.4791	46 ± 2
	100724A	1.288	16.4 ± 2.4	131103A	0.599	19.9 ± 2.2
	101219A	0.718	48.8 ± 6.8	140318A	1.02	15.1 ± 4.9
	120804A	1.3	70.0 ± 15.0	140710A	0.558	7.34 ± 0.96
	130603B	0.356	21.2 ± 2.3	150818A	0.282	13.91 ± 4.59
	140622A	0.959	0.70 ± 0.13	150915A	1.968	9.95 ± 2.24
	140903A	0.351	1.41 ± 0.11	151029A	1.423	28.4 ± 14.8
	101225A	0.847	26 ± 20	151031A	1.167	76.3 ± 7.1
	111005A	0.013	0.0088 ± 0.0016	160117B	0.870	34.0 ± 0.4
	111129A	1.0796	52 ± 12	160314A	0.726	32.0 ± 4.6
	111225A	0.297	3.55 ± 0.56	160425A	0.555	71.0 ± 6.8
	111229A	1.3805	9.0 ± 1.2	161219B	0.1475	2.33 ± 0.74
120121B	0.017	0.0139 ± 0.0002				

Group	XRF	z	E_p (keV)	E_{iso} (10^{50} erg)	<i>Fermi</i> GCN	θ (deg)	GeV observed
Outside Boresight	110106B	0.618	209.851	73 ± 4	GCN 11543	103	no
	120907A	0.97	304.365	20.1 ± 2.8	GCN 13721	110	no
	Angle	130612A	2.006	186.07	71.7 ± 7.6	GCN 14896	—
Inside Boresight	101219B	0.55	108.50	63 ± 6	GCN 11477	59	no
Angle	121211A	1.023	194.00	61 ± 22	GCN 14078	74	no
Angle	140606B	0.384	654.63	39.9 ± 1.6	GCN 16363	66	no
Angle	150727A	0.313	195.054	19.52 ± 2.56	GCN 18081	46	no

Table 3

List of 48 X-ray flashes (XRFs) divided in three different groups, the one without *Fermi*-LAT observation (upper group), with the *Fermi*-LAT observation but the boresight $\theta \geq 75^\circ$, the one within the *Fermi*-LAT boresight angle (lower group, $\theta < 75^\circ$), none of the S-GRFs have any GeV photon detected. In the first column we indicate the name of the sources, in the second their redshift, in third column we indicate the $E_{p,i}$ only deducible from the *Fermi* data, in the fourth column we estimate E_{iso} which is systematically lower than the 10^{52} erg, we also add for convenience both the specific GCN of the *Fermi* source as well as the boresight angle of the LAT observation in the column of the the non-observation of the GeV emission. The symbol “—” indicates no information on LAT boresight angle due to lack of GBM observation.

χ^2 represents the difference between the best power-laws fitting and all the observed data, it is a summation of individual χ_n^2 , which represents the difference between the power-law fitting and the observed value of each GRB.

Out of 21 BdHNe presented in Table 4 we perform the fitting for only 17 GRBs which have more than two data points in their luminosity light-curves. Therefore, for the fitting of BdHNe, there are 17 bursts and each one has its power-law function. Consequently, there are in total 17 parameters, including 17 amplitudes, and 1 power-law index. The fitting gives the power-law index $\alpha = 1.2 \pm 0.04$, i.e.:

$$L_n = A_n t^{-1.2 \pm 0.04}, \quad (4)$$

which is plotted in Fig. 1 and the amplitudes of each GRB, A_n , with the uncertainty are shown in Table 5.

After having the best power-law parameters of the light curve for each BdHNe, we check the correlation between the GeV luminosity at 10 s from Eq. (4) using the fitted parameters and the isotropic energy E_{iso} . The power-law fitting gives (see Fig. 2):

$$L_{10s} = (3.701 \pm 2.21) \times 10^{51} E_{\text{iso}}^{1.428 \pm 0.425}, \quad (5)$$

and the fitting parameters for each GRB including their uncertainties are shown in Table 5. Furthermore, we

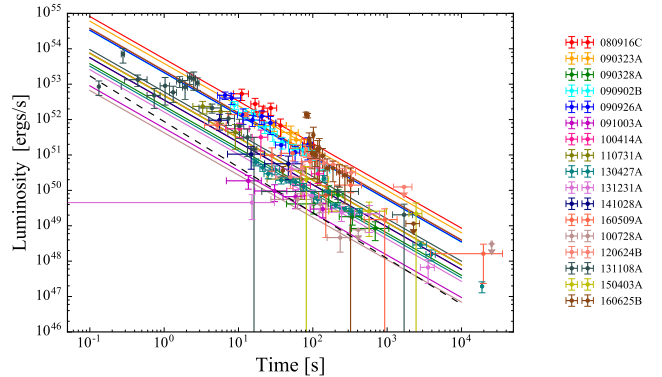


Figure 1. The rest-frame 0.1–100 GeV isotropic luminosity light-curves of 17 selected BdHNe with LAT emission. The solid red line marks the common power-law behavior of the GeV emission for BdHNe with slope $\alpha = 1.20 \pm 0.04$; the shaded gray area encloses all the luminosity light-curves of the selected BdHNe. The dashed black line marks the common power-law behavior of the GeV emission in S-GRBs with slope $\gamma = 1.29 \pm 0.06$.

estimate the energy released in the GeV band by each GRB in the $0.1\text{--}10^4$ s time interval, i.e.:

$$E_{0.1-10^4s} = A_{\text{GRB}} \int_{0.1}^{10000} t^{-1.19} dt \quad (6)$$

Source	z	$E_{p,i}$ (MeV)	E_{iso} (10^{52} erg)	Fermi GCN	E_{LAT} (10^{52} erg)	θ (deg)	TS	Comments
BdHN 080916C	4.35	2.27 ± 0.13	407 ± 86	GCN 8246	$\gtrsim 408 \pm 57$	48.8	1450	
BdHN 090323A	3.57	2.9 ± 0.7	438 ± 53	GCN 9021	$\gtrsim 48.85 \pm 0.59$	57.2	150	
BdHN 090328A	0.736	1.13 ± 0.08	14.2 ± 1.4	GCN 9044	$\gtrsim 3.04 \pm 0.01$	64.6	107	
BdHN 090902B	1.822	2.19 ± 0.03	292 ± 29.2	GCN 9867	$\gtrsim 110 \pm 5$	50.8	1832	
BdHN 090926A	2.106	0.98 ± 0.01	228 ± 23	GCN 9934	$\gtrsim 151 \pm 7$	48.1	1983	
BdHN 091003A	0.897	0.92 ± 0.04	10.7 ± 1.8	GCN 9985	$\gtrsim 1.29 \pm 0.03$	12.3	108	
BdHN 091208B	1.063	0.25 ± 0.04	2.10 ± 0.11	GCN 10266	$\gtrsim 0.41 \pm 0$	55.6	20	
BdHN 100414A	1.368	1.61 ± 0.07	55.0 ± 0.5	GCN 10594	$\gtrsim 8.79 \pm 0.31$	69	81	
BdHN 100728A	1.567	1.00 ± 0.45	72.5 ± 2.9	GCN 11006	$\gtrsim 1.15 \pm 0.2$	59.9	32	
BdHN 110731A	2.83	1.21 ± 0.04	49.5 ± 4.9	GCN 12221	$\gtrsim 31.4 \pm 7.4$	3.4	460	
BdHN 120624B	2.197	1.39 ± 0.35	347 ± 16	GCN 13377	$\gtrsim 28 \pm 2$	70.8	312	
BdHN 130427A	0.334	1.11 ± 0.01	92 ± 13	GCN 14473	$\gtrsim 5.69 \pm 0.05$	47.3	163	
BdHN 130518A	2.488	1.43 ± 0.38	193 ± 1	GCN 14675	$\gtrsim 3.5 \pm 0.6$	41.5	50	
BdHN 131108A	2.40	1.27 ± 0.05	51.2 ± 3.83	GCN 15464	$\gtrsim 50.43 \pm 5.86$	23.78	870	
BdHN 131231A	0.642	0.27 ± 0.01	21.50 ± 0.02	GCN 15640	$\gtrsim 2.18 \pm 0.02$	38	110	
BdHN 141028A	2.33	0.77 ± 0.05	76.2 ± 0.6	GCN 16969	$\gtrsim 7.36 \pm 0.46$	27.5	104.5	
BdHN 150314A	1.758	0.86 ± 0.01	70.1 ± 3.25	GCN 17576	$\gtrsim 1.93 \pm 0.89$	47.13	27.1	
BdHN 150403A	2.06	0.95 ± 0.04	87.3 ± 7.74	GCN 17667	$\gtrsim 7.55 \pm 5.19$	55.2	37	
BdHN 150514A	0.807	0.13 ± 0.01	1.14 ± 0.03	GCN 17816	$\gtrsim 0.42 \pm 0.05$	38.5	33.9	
BdHN 160509A	1.17	0.80 ± 0.02	84.5 ± 2.3	GCN 19403	$\gtrsim 35.92 \pm 0.26$	32	234	
BdHN 160625B	1.406	1.3 ± 0.1	337 ± 1	GCN 19581, GCN19604	$\gtrsim 29.90 \pm 3.51$	41.46	961.33	

Table 4

List of 21 BdHNe inside Fermi-LAT boresight angle and GeV photon detected: the prompt and GeV emission properties of 21 BdHNe with GeV emission detected. Columns list: the source name, z , $E_{p,i}$, E_{iso} , E_{LAT} , the position of the source from the LAT boresight θ , the likelihood test statistic (TS). The E_{LAT} includes only the energy in the observed time duration, which does not cover the whole GeV emission period, and is different for each GRB, so we put a symbol ' \gtrsim ' to indicate the value is the lower limit.

BdHNe	A_n (Amplitude)	uncertainty of A_n	L_{10s}	uncertainty of L_{10s}
080916C	5.201×10^{53}	$+1.605$ -1.307×10^{53}	3.341×10^{52}	$+1.963$ -1.800×10^{52}
090323A	3.847×10^{53}	$+1.436$ -1.169×10^{53}	2.472×10^{52}	$+1.542$ -1.397×10^{52}
090328A	2.408×10^{52}	$+1.087$ -0.773×10^{52}	1.547×10^{51}	$+1.042$ -0.889×10^{51}
090902B	2.091×10^{53}	$+5.845$ -4.599×10^{53}	1.343×10^{52}	$+7.696$ -7.055×10^{51}
090926A	2.141×10^{53}	$+5.887$ -4.838×10^{53}	1.376×10^{52}	$+7.850$ -7.259×10^{51}
091003A	5.715×10^{51}	$+1.735$ -1.520×10^{51}	3.671×10^{50}	$+2.004$ -2.147×10^{50}
100414A	3.529×10^{52}	$+1.399$ -1.142×10^{52}	2.267×10^{51}	$+1.446$ -1.306×10^{51}
110731A	4.807×10^{52}	$+1.707$ -1.442×10^{52}	3.088×10^{51}	$+1.894$ -1.739×10^{51}
130427A	2.053×10^{52}	$+5.124$ -4.091×10^{52}	1.318×10^{51}	$+7.370$ -6.815×10^{50}
131231A	1.637×10^{52}	$+7.818$ -5.446×10^{52}	1.052×10^{51}	$+7.273$ -6.116×10^{50}
141028A	3.590×10^{52}	$+1.225$ -1.109×10^{52}	2.306×10^{51}	$+1.396$ -1.310×10^{51}
160509A	4.812×10^{52}	$+1.733$ -1.313×10^{52}	3.091×10^{51}	$+1.905$ -1.698×10^{51}
100728A	4.241×10^{51}	$+1.978$ -1.512×10^{51}	2.725×10^{50}	$+1.863$ -1.622×10^{50}
120624B	2.459×10^{53}	$+8.261$ -6.167×10^{53}	1.580×10^{52}	$+9.518$ -8.513×10^{51}
131108A	6.077×10^{52}	$+9.089$ -8.894×10^{52}	3.904×10^{51}	$+2.037$ -1.947×10^{51}
150403A	4.671×10^{52}	$+2.034$ -1.595×10^{52}	3.001×10^{51}	$+1.989$ -1.760×10^{51}
160625B	2.378×10^{53}	$+8.093$ -5.854×10^{53}	1.528×10^{52}	$+9.241$ -8.199×10^{51}

Table 5

Fitting parameters of the relation between 0.1–100 GeV luminosity vs. time when measured in the rest frame of 17 BdHNe with GeV emission: amplitude of the BdHNe 0.1–100 GeV luminosity, A_n , and its uncertainty, the inferred 0.1–100 GeV luminosity at 10 s from the fitting and its uncertainty. The common power-law index is $\alpha = 1.20 \pm 0.04$. Out of 21 BdHNe emitting GeV emission we performed the fitting for 17 GRBs which have more than two data points in their luminosity light-curves.

and the derived $E_{0.1-10^4s}$ are shown in Table 6. The parameters $E_{0.1-10^4s}$ and E_{iso} (isotropic energy of the prompt emission in γ band) are also correlated by a power-law relation (see Fig. 3):

$$E_{0.1-10^4s} = (4.125 \pm 2.59) \times 10^{53} E_{iso}^{1.424 \pm 0.447}. \quad (7)$$

This positive correlations indicates that the BdHNe with higher isotropic energy are also more luminous and more energetic in the GeV emission.

We can now proceed to the corresponding analysis already performed for determination of the mass of the

BH.

5. THE DETERMINATION OF THE MASS OF THE BH IN BDHNE

The first proposal for explaining the origin of the GeV energetics and for constraining the mass and spin of Kerr BH was introduced in Ruffini et al. (2018b) for S-GRBs. We here use the same procedure for the case of BdHNe.

The extractable energy of a Kerr BH, E_{extr} , is given

BdHNe	$E_{0.1-10^4 s}$	positive uncertainty of $E_{0.1-10^4 s}$	negative uncertainty of $E_{0.1-10^4 s}$
080916C	3.752×10^{54}	1.460×10^{54}	1.242×10^{54}
090323A	2.775×10^{54}	1.227×10^{54}	1.034×10^{54}
090328A	1.737×10^{53}	8.860×10^{52}	6.723×10^{52}
090902B	1.508×10^{54}	5.529×10^{53}	4.646×10^{53}
090926A	1.545×10^{54}	5.608×10^{53}	4.824×10^{53}
091003A	4.122×10^{52}	1.588×10^{52}	1.411×10^{52}
100414A	2.546×10^{53}	1.176×10^{53}	9.902×10^{52}
100728A	3.060×10^{52}	1.600×10^{52}	1.275×10^{52}
110731A	3.467×10^{53}	1.481×10^{53}	1.281×10^{53}
120624B	1.774×10^{54}	7.294×10^{53}	5.867×10^{53}
130427A	1.481×10^{53}	5.098×10^{52}	4.348×10^{52}
131108A	4.383×10^{53}	1.228×10^{53}	1.142×10^{53}
131231A	1.181×10^{53}	6.297×10^{52}	4.682×10^{52}
141028A	2.589×10^{53}	1.076×10^{53}	9.757×10^{52}
150403A	3.369×10^{53}	1.671×10^{53}	1.361×10^{53}
160509A	3.471×10^{53}	1.497×10^{53}	1.207×10^{53}
160625B	1.716×10^{54}	7.116×10^{53}	5.614×10^{53}

Table 6
Results of $E_{0.1-10^4 s}$ and related error of 20 BdHNe. $E_{0.1-10^4 s}$ is total GeV energy (in erg) emitted from 0.1 to 10^4 s.

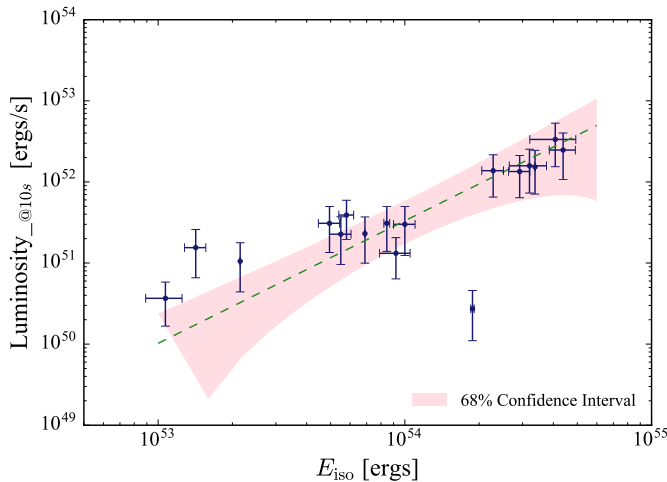


Figure 2. The *Fermi*-LAT luminosity at 10s in the energy range 0.1–100 GeV versus the isotropic gamma-ray energy from 1 keV to 10 MeV. The BdHNe are listed in Table 4.

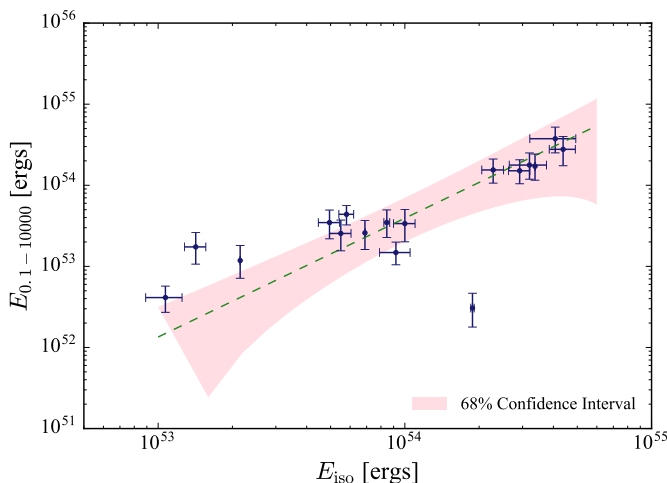


Figure 3. The *Fermi*-LAT energy from 0.1 to 10^4 second versus isotropic gamma-ray energy from 1 keV to 10 MeV.

by (Ruffini et al. 2018b)

$$E_{\text{extr}} = M - M_{\text{irr}} = \left(1 - \sqrt{\frac{1 + \sqrt{1 - \alpha^2}}{2}}\right) M, \quad (8)$$

in which $\alpha = J/M^2$ (the spin parameter) is the dimensionless intrinsic angular momentum and M and M_{irr} are respectively the mass and the irreducible mass of a Kerr BH. Requesting the condition that observed GeV emission originates from BH extractable energy, namely $E_{\text{LAT}} = E_{\text{extr}}$, we can then obtain M as a function of α , $M(\alpha)$.

On the other hand, we have that the NS critical mass value, for the NL3, GM1 and TM1 equation of state (EOS) is fitted, with a maximum error of 0.45%, by the following relation (Cipolletta et al. 2015)

$$M_{\text{crit}}(\alpha) = M_{\text{crit}}^{J=0}(1 + kj^p), \quad (9)$$

where k and p are parameters that depend upon the nuclear EOS, $M_{\text{crit}}^{J=0}$ is the critical mass in the non-rotating (spinless) case and j is the dimensionless angular momentum parameter $j \equiv \alpha(M_{\text{crit}}/M_{\odot})^2$. More details can be seen in Cipolletta et al. (2015) and Ruffini et al. (2018b).

Since in BdHNe the BH is formed in a hypercritical accretion onto a NS we request the mass of the BH to satisfy $M \geq M_{\text{crit}}(\alpha)$. In 16 BdHNe out of the 21 ones in Table 4, the minimum BH mass, and corresponding maximum BH spin parameter are respectively in the range of $2.21 \leq M \leq 2.64 M_{\odot}$ and $0.05 \leq \alpha \leq 0.71$, for the TM1 model, and $2.81 \leq M \leq 3.23 M_{\odot}$ and $0.04 \leq \alpha \leq 0.65$, for the NL3 model. In both cases, these mass ranges are almost similar to those obtained in S-GRBs however the spin ranges are wider see Table 5 in Ruffini et al. (2018b) and Table 7.

6. BLACK HOLE & HYPERNOVA BINARY (BH-HN)

In 5 BdHNe out of the 21 ones in Table 4, the limitation of $M \geq M_{\text{crit}}(\alpha)$, implicitly introduced by Eq. 9, leads to $\alpha \geq \alpha_{\text{max}}$. Therefore, for these 5 BdHNe we fix $\alpha \equiv \alpha_{\text{max}}$ and we compute the BH mass M necessary to explain the values E_{LAT} in Table 4. These minimum masses are listed in the Table 8 and range in the interval

Source	TM1		NL3	
	α	$M(\alpha)$ (M_{\odot})	α	$M(\alpha)$ (M_{\odot})
BdHN 090328A	$0.2434^{+0.0004}_{-0.0004}$	$2.2526^{+0.0001}_{-0.0001}$	$0.2167^{+0.0003}_{-0.0003}$	$2.8538^{+0.0001}_{-0.0001}$
BdHN 091003A	$0.161^{+0.002}_{-0.002}$	$2.2259^{+0.0005}_{-0.0005}$	$0.143^{+0.001}_{-0.001}$	$2.8311^{+0.0004}_{-0.0004}$
BdHN 091208B	$\lesssim 0.0910$	$\gtrsim 2.2101$	$\lesssim 0.0806$	$\gtrsim 2.818$
BdHN 100414A	$0.400^{+0.006}_{-0.006}$	$2.330^{+0.004}_{-0.004}$	$0.359^{+0.006}_{-0.006}$	$2.921^{+0.003}_{-0.003}$
BdHN 100728A	$0.1516^{+0.0124}_{-0.0136}$	$2.2235^{+0.0033}_{-0.0034}$	$0.1345^{+0.0111}_{-0.0121}$	$2.8291^{+0.0028}_{-0.00286}$
BdHN 110731A	$0.68^{+0.05}_{-0.06}$	$2.57^{+0.12}_{-0.10}$	$0.62^{+0.05}_{-0.06}$	$3.18^{+0.09}_{-0.09}$
BdHN 120624B	$0.6429^{+0.0154}_{-0.0167}$	$2.5966^{+0.0320}_{-0.0307}$	$0.5930^{+0.0160}_{-0.0170}$	$3.1362^{+0.0236}_{-0.0232}$
BdHN 130427A	$0.327^{+0.001}_{-0.001}$	$2.2893^{+0.0006}_{-0.0006}$	$0.293^{+0.001}_{-0.001}$	$2.8854^{+0.0005}_{-0.0005}$
BdHN 130518A	$0.2604^{+0.0204}_{-0.0224}$	$2.2592^{+0.0084}_{-0.0086}$	$0.2320^{+0.0184}_{-0.0202}$	$2.8594^{+0.0073}_{-0.0074}$
BdHN 131231A	$0.2075^{+0.0007}_{-0.0007}$	$2.2399^{+0.0002}_{-0.0002}$	$0.1844^{+0.0006}_{-0.0006}$	$2.8430^{+0.0002}_{-0.0002}$
BdHN 141028A	$0.37^{+0.01}_{-0.01}$	$2.312^{+0.006}_{-0.006}$	$0.331^{+0.009}_{-0.010}$	$2.905^{+0.005}_{-0.005}$
BdHN 150314A	$0.1954^{+0.0395}_{-0.0511}$	$2.2360^{+0.0133}_{-0.0144}$	$0.1736^{+0.0354}_{-0.0456}$	$2.8397^{+0.0114}_{-0.0122}$
BdHN 150403A	$0.3734^{+0.0976}_{-0.1580}$	$2.3141^{+0.0679}_{-0.0716}$	$0.3348^{+0.0907}_{-0.1432}$	$2.9067^{+0.0578}_{-0.0615}$
BdHN 150514A	$0.0921^{+0.0053}_{-0.0056}$	$2.2103^{+0.0010}_{-0.0010}$	$0.0816^{+0.0047}_{-0.0050}$	$2.8181^{+0.0008}_{-0.0008}$
BdHN 160509A	$0.707^{+0.002}_{-0.002}$	$2.636^{+0.004}_{-0.004}$	$0.651^{+0.002}_{-0.002}$	$3.232^{+0.003}_{-0.003}$
BdHN 160625B	$0.6576^{+0.0244}_{-0.0280}$	$2.6270^{+0.0598}_{-0.0552}$	$0.6082^{+0.0259}_{-0.0288}$	$3.1586^{+0.0424}_{-0.0412}$

Table 7

The BH spin parameter α and mass M within the TM1 and the NL3 nuclear models, as inferred from the values of E_{LAT} for 16 BdHNe, out of the 21 ones in Table. 4, providing BH spin parameters $\alpha < 0.71$, consistent with the maximum spin parameter of a rotating NS (see Cipolletta et al. 2015, for details).

Source	α	$M(\alpha)$ (M_{\odot})
BdHN 080916C	0.71	29.7 ± 3.4
BdHN 090323A	0.71	3.55 ± 0.04
BdHN 090902B	0.71	7.99 ± 0.36
BdHN 090926A	0.71	10.98 ± 0.51
BdHN 131108A	0.71	3.67 ± 0.43

Table 8

The 5 BdHNe, out of the 21 ones in Table. 4, requiring $M > M_{\text{max}}^{J=0}$. The masses M have been obtained from Eq. 4 in Ruffini et al. (2018b) by fixing $\alpha = \alpha_{\text{max}}$.

$3.55 \leq M \leq 29.7 M_{\odot}$. Such values are higher than those attainable in normal BdHNe where the NS binary companion collapses into a BH with a mass value close to the NS critical mass. This fact finds a natural explanation whether the progenitor system is a CO_{core}-BH binary instead of a CO_{core}-NS binary. This possibility has been already advanced in Ruffini et al. (2016b) and Ruffini et al. (2016c) and finds here a further confirmation. Unlike the case of the S-GRBs there are clearly two sets of the systems in the case of BdHNe: 1) the first family with BH mass close to the critical mass of the NS, see Table 7. It is interesting to notice that the mass of the newly born BH in this system is very similar to the one observed in S-GRBs see Table 5 in (Ruffini et al. 2018b). 2) the second family with systematically larger masses all the way up to $29 M_{\odot}$ which cannot be envisaged to Kerr BH in the accretion in the second subclass of BdHN, but most likely the third class of GRBs namely the one with BH-HN progenitor.

7. BDHN WITHOUT GEV EMISSION AND GEOMETRY OF THE BDHNE

The unexpected result has been the presence of 27 BdHNe within the LAT boresight but not GeV emission detection, see Table 9. What is extremely interesting is that, although the distribution of the angle, redshift, $E_{\text{p},i}$, E_{LAT} and E_{iso} is totally analogous to the of the BdHNe examined, no GeV emission is observed.

This subclass of BdHNe are identifying as the sources of X-Ray and Gamma-ray flare episodes as recently was discussed in the case of GRB 151027A in Ruffini et al. (2017), see also Nappo et al. (2017).

To constrain the geometry of the region from which the GeV photons are emitted, we look at the ratio between the number of GRBs emitting GeV emission N_{LAT} , and the total number of GRBs N_{tot} within the LAT FoV. Assuming a two-side cone emitting region, the half-opening angle of a single cone ϑ is given by

$$1 - \cos \vartheta = \frac{N_{\text{LAT}}}{N_{\text{tot}}}. \quad (10)$$

In the case of S-GRBs we have seen that $N_{\text{LAT}} \equiv N_{\text{tot}}$ (see Table 4 of Ruffini et al. (2018b)) and therefore their GeV emission is spherically symmetric. For BdHNe, our search in the LAT data¹⁰ gives $N_{\text{LAT}} = 21$ and $N_{\text{tot}} = 48$, leading to $\vartheta = 55.77^\circ$. Therefore, in BdHNe the GeV emission comes from a wide angle emission as can be seen in idealized Fig. 4. Therefore, the following general conclusion can be reached: 1) In S-GRBs the GeV emission is not obstructed by surrounding matter, and consequently, a clear isotropic emission is observed. This has been interpreted as the merging of the two NSs leading to the direct formation of BH, unimpeded by surrounding matter. 2) In the case of BdHNe a clear different morphology is present due to the well tested theory conceptually and visibly represented by a large number of numerical simulations describing the accretion of the SN ejected material around the NS companion, see Fig. 5 and its idealized representation in Fig. 4.

What can be concluded from the above results is that in BdHNe, in view of the ejected SN accreting material, the GeV emission released only normal to the orbital plane of the binary and it is only detectable when the viewing angle is less than the $\approx 60^\circ$ from the normal to the plane, see left plot in Fig. 4. Whenever the viewing

¹⁰ https://fermi.gsfc.nasa.gov/ssc/observations/types/grbs/lat_grbs/table.php

BdHNe	z	E_p (MeV)	E_{iso} (10^{52} erg)	Fermi GCN	θ (deg)	GeV observed	comments
081222	2.77	0.51 ± 0.03	27.4 ± 2.7	GCN 8715	50.0	no	
090424A	0.544	0.27 ± 0.04	4.07 ± 0.41	GCN 9230	71.0	no	
090516A	4.109	0.14 ± 0.03	99.6 ± 16.7	GCN 9415	20.0	no	Clear X-ray flare observed
091127A	0.49	0.05 ± 0.01	1.64 ± 0.18	GCN 10204	25.0	no	
100615A	1.398	0.21 ± 0.02	5.81 ± 0.11	GCN 10851	64.0	no	
100728B	2.106	0.32 ± 0.04	3.55 ± 0.36	GCN 11015	57.1	no	
110128A	2.339	0.46 ± 0.01	1.58 ± 0.21	GCN 11628	45.0	no	
111228A	0.716	0.060 ± 0.007	2.75 ± 0.28	GCN 12744	70.0	no	
120119A	1.728	0.52 ± 0.02	27.2 ± 3.6	GCN 12874	31.4	no	
120712A	4.175	0.64 ± 0.13	21.2 ± 2.1	GCN 13469	42.0	no	
120716A	2.486	0.4 ± 0.04	30.2 ± 3.0	GCN 13498	63.0	no	
120909A	3.93	0.87 ± 0.01	87 ± 10	GCN 13737	66.0	no	
130528A	1.250	0.27 ± 0.18	18.01 ± 2.28	GCN 14729	60.0	no	X-ray flare observed
130925A	0.347	0.14 ± 0.04	3.23 ± 0.37	GCN 15261	22.0	no	X-ray flare observed
131105A	1.686	0.55 ± 0.08	34.7 ± 1.2	GCN 15455	37.0	no	
140206A	2.73	1.1 ± 0.03	144.24 ± 19.20	GCN 15790	46.0	no	Clear X-ray flare observed
140213A	1.2076	0.176 ± 0.004	9.93 ± 0.15	GCN 15833	48.5	no	
140423A	3.26	0.53 ± 0.04	65.3 ± 3.3	GCN 16152	44.0	no	
140623A	1.92	1.02 ± 0.64	7.69 ± 0.68	GCN 16450	32.0	no	
140703A	4.13	0.91 ± 0.07	1.72 ± 0.09	GCN 16512	16.0	no	
140907A	1.21	0.25 ± 0.02	2.29 ± 0.08	GCN 16798	16.0	no	X-ray flare observed
141220A	1.3195	0.42 ± 0.02	2.44 ± 0.07	GCN 17205	47.0	no	
150301B	1.5169	0.45 ± 0.10	2.87 ± 0.42	GCN 17525	39.0	no	
150821A	0.755	0.57 ± 0.03	14.7 ± 1.1	GCN 18190	57.0	no	
151027A	0.81	0.62 ± 0.11	3.94 ± 1.33	GCN 18492	10.0	no	Clear X-ray flare observed
151111A	3.5	0.25 ± 0.04	3.43 ± 1.19	GCN 18582	50.0	no	X-ray flare observed
161014A	2.823	0.64 ± 0.06	10.1 ± 1.7	GCN 20051	69.0	no	

Table 9

List of 27 BdHNe inside Fermi-LAT boresight angle and no GeV photon detected: 27 BdHNe with redshift taken from (Ruffini et al. 2016b) from 2008, when Fermi started to operate, till the end of 2016. All of them are within the boresight of Fermi-LAT, but none detected GeV photon. For each source the columns list: z , E_{iso} , E_p , GCN number, position of the source from LAT boresight θ , whether was detection by LAT, and additional information.

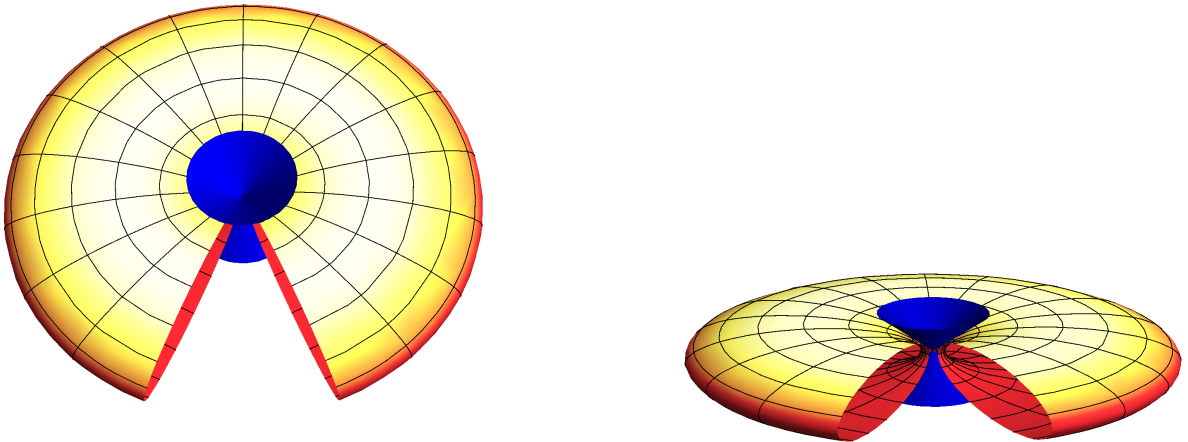


Figure 4. Idealized plot for showing the morphology of the BdHNe. The GeV emission is detectable when the viewing angle is less than the 55.77° from the normal to the orbital plane. Left panel is the situation in which the detectors can observe the GeV emission and the right panel is the one which GeV emission is not detectable and only Gamma-ray and X-ray flares are detectable.

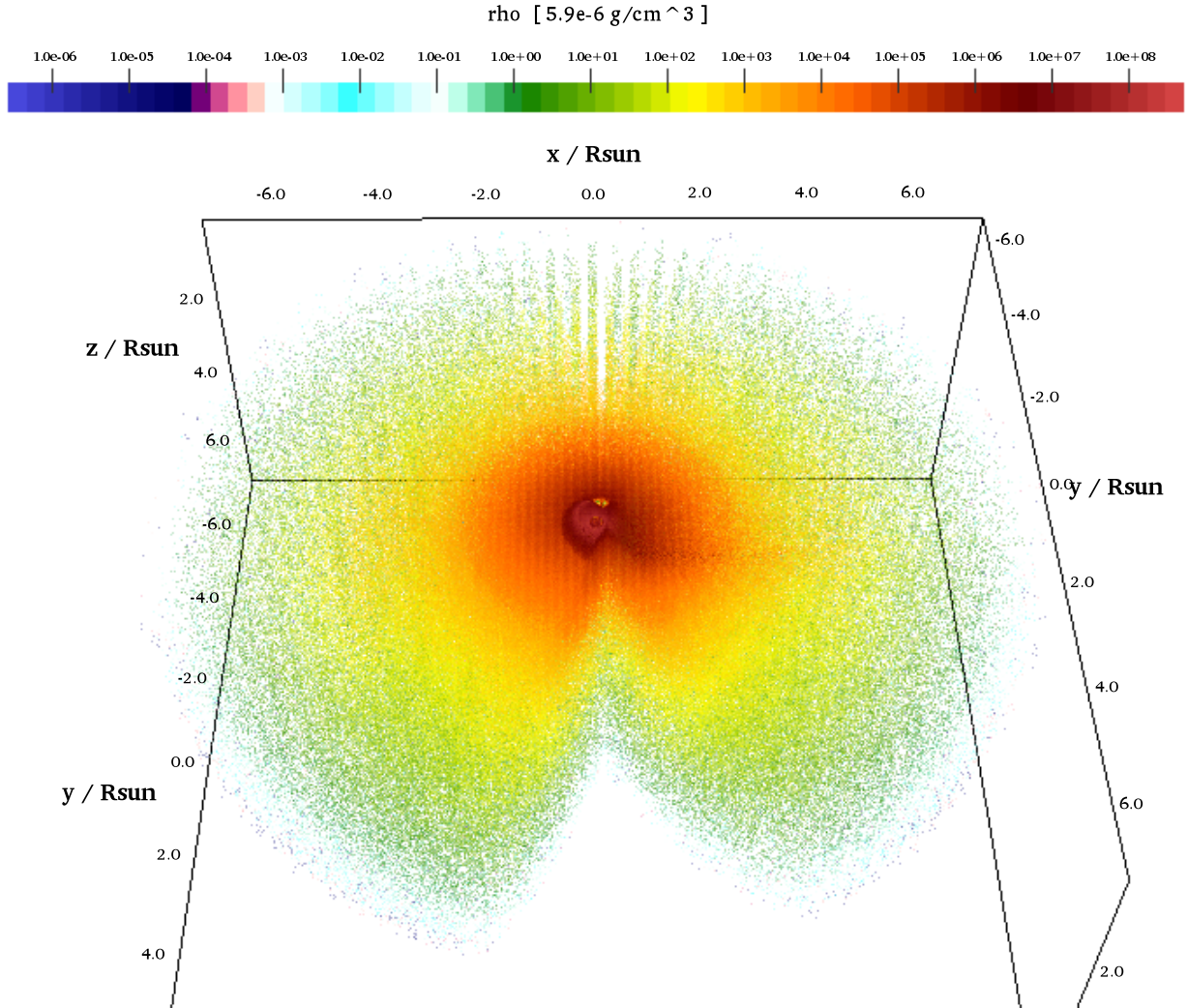


Figure 5. Three-dimensional, half hemisphere views of the density distribution of the SN ejecta at the moment of BH formation in a BdHN. The simulation is performed with a SPH code that follows the SN ejecta expansion under the influence of the NS companion gravitational field including the effects of the orbital motion and the changes in the NS gravitational mass by the hypercritical accretion process. The initial conditions of the SN ejecta are set by a homologous velocity distribution in free expansion and the mass-distribution is modeled with 16 millions point-like particles (see Becerra et al. 2016, for additional details). The binary parameters of this simulation are: the NS companion has an initial mass of $2.0 M_{\odot}$; the CO_{core} , obtained from a progenitor with ZAMS mass $M_{\text{ZAMS}} = 30 M_{\odot}$, leads to a total ejecta mass $7.94 M_{\odot}$ and to a $1.5 M_{\odot} \nu\text{NS}$, the orbital period is $P \approx 5$ min (binary separation $a \approx 1.5 \times 10^{10}$ cm).

angle is within 60° from the co-planarity condition no GeV emission is observed though X-ray and Gamma-ray Flares are observed, see right plot in Fig. 4.

8. SPH SIMULATION OF BDHNE

The numerical simulation at the moment of BH formation in a BdHN is presented in Becerra et al. (2016, 2018a). Three-dimensional (3D) views of the density distribution at the moment of the BH formation in a BdHN are shown Fig. 5. These plots correspond to the simulation of the SN ejecta expansion under the presence of the NS companion. The simulation is performed with a SPH technique in which the SN ejecta material is divided by N point-like particles, in the present case 16 million, with different masses and followed their motion under the NS gravitational field. The orbital motion of the NS around the SN explosion center is taking into account as well as the NS star gravitational mass changes via the hypercritical accretion process. The last was modeled independently estimating the accretion rate on the NS with the Bondi-Hoyle formalism. For the initial conditions of the simulation was adopted a homologous velocity distribution in free expansion and the power law initial density profile of the SN matter was modeled by populating the inner layers with more particles (see Becerra et al. 2016, 2018a, for additional details). Figure. 5 corresponds to an initial binary system formed by a $2 M_\odot$ NS and the CO_{core} , obtained from a progenitor with $M_{\text{ZAMS}} = 30 M_\odot$. When the CO_{core} collapses and explodes, ejects $7.94 M_\odot$ and leads a νNS of $1.5 M_\odot$. The initial binary period is about 5 min ($\approx 1.5 \times 10^{10}$ cm).

9. CONCLUSIONS

We have used the GeV emission as an additional tool to discriminate between XRF and BdHN. This follows the previously identified differences in their spectra and energetics (XRF: with $E_{\text{p,i}} \sim 0.004\text{--}0.3$ MeV and $E_{\text{iso}} \sim 10^{48}\text{--}10^{52}$ erg and BdHN: with $E_{\text{p,i}} \sim 0.2\text{--}2$ MeV and $E_{\text{iso}} \sim 10^{52}\text{--}10^{54}$ erg). From 48 BdHNe we identify two subclasses, 21 emitting GeV radiation and 27 with X-ray and Gamma-ray flaring activities with not emitting GeV radiation. To the BdHNe having the GeV emission the relation between the 0.1–100 GeV luminosity light-curve versus time in the rest frame of the GRBs shows the universal power-law: $L_n = A_n t^{-1.20 \pm 0.04}$ erg s $^{-1}$, the power-law index is similar to the one discovered in S-GRBs, -1.29 ± 0.06 . While in S-GRBs the amplitude, A_n , is universal, in the case of BdHNe the amplitude is strongly dependent on the isotropic energy of the source.

We further inferred that the GeV emission gives necessary condition for the formation of the BH in the hypercritical accretion of HN onto the companion NS: in turn the presence of the BH is sufficient to explain the energy of the GeV emission. By using the mass formula of the BH we infer that there are two sets of systems in the BdHNe: 1) the first with BH minimum mass near the NS critical mass in the range of $2.21 \leq M \leq 3.23 M_\odot$ and 2) the second with larger minimum mass all the way up to the $29 M_\odot$, which is associated with the new class of GRBs with BH-HN progenitor system. On the ground of the result that in S-GRBs the GeV emission is always present we infer its wide angle leading to a nearly isotropic emission. In the case of BdHN the presence of the HN ejecta confines the GeV emission to be detectable

only when emitted in a double conical region normal to the BdHN orbital plane by approximately 60° : namely, when the GRB line-of-sight forms an angle of less than 60° with the normal to the BdHN orbital plane the GeV emission is observable. In the opposite case, only the prompt emission phase and the gamma-ray flares and the X-ray flares are observable. We infer that in BdHNe a morphology very similar to the one observed in AGNs, although on a smaller scale, in view of the stellar mass BH, also with less spatial symmetries, in absence of a perfect rotational symmetry, and temporal symmetry, in view of the transient nature of the event.

We acknowledge the continuous support of the MAECI. This work made use of data from Fermi space observatory. Y. A. is supported by the Erasmus Mundus Joint Doctorate Program Grant N. 2014-0707 from EACEA of the European Commission. Y. A. acknowledges partial support by the Targeted Financing Program BR05336383 of Aerospace Committee of the Ministry of Defense and Aerospace Industry of the Republic of Kazakhstan. G. J. M is supported by the U.S. Department of Energy under Nuclear Theory Grant DE-FG02-95-ER40934. M. M. acknowledges partial support provided by a targeted funding for scientific and technical program of the Ministry of Education and Science of Kazakhstan.

REFERENCES

- Ackermann, M., Ajello, M., Asano, K., et al. 2013, *ApJS*, 209, 11
 Aimuratov, Y., Ruffini, R., Muccino, M., et al. 2017, *ApJ*, 844, 83
 Becerra, L., Bianco, C. L., Fryer, C. L., Rueda, J. A., & Ruffini, R. 2016, *ApJ*, 833, 107
 Becerra, L., Cipolletta, F., Fryer, C. L., Rueda, J. A., & Ruffini, R. 2015, *ApJ*, 812, 100
 Becerra, L., Ellinger, C. L., Fryer, C. L., Rueda, J. A., & Ruffini, R. 2018a, *ArXiv e-prints*
 Becerra, L., Guzzo, M. M., Rossi-Torres, F., et al. 2018b, *ApJ*, 852, 120
 Bromberg, O., Nakar, E., Piran, T., & Sari, R. 2013, *ApJ*, 764, 179
 Cipolletta, F., Cherubini, C., Filippi, S., Rueda, J. A., & Ruffini, R. 2015, *Phys. Rev. D*, 92, 023007
 Della Valle, M. 2011, *International Journal of Modern Physics D*, 20, 1745
 Fryer, C. L., Oliveira, F. G., Rueda, J. A., & Ruffini, R. 2015, *Physical Review Letters*, 115, 231102
 Fryer, C. L., Rueda, J. A., & Ruffini, R. 2014, *ApJ*, 793, L36
 Gill, P. R.; Murray, W., & Wright, M. H. 1981, 500, 136
 Hjorth, J., & Bloom, J. S. 2012, *Cambridge Astrophysics Series*, Vol. 51, *The Gamma-Ray Burst - Supernova Connection*, ed. C. Kouveliotou, R. A. M. J. Wijers, & S. Woosley (Cambridge University Press (Cambridge)), 169–190
 Izzo, L., Ruffini, R., Penacchioni, A. V., et al. 2012, *A&A*, 543, A10
 Lyman, J. D., Bersier, D., James, P. A., et al. 2016, *MNRAS*, 457, 328
 MacFadyen, A., & Woosley, S. E. 1999, *ApJ*, 524, 262 P., & Rees, M. J. 1992a (*ApJ*)
 Nappo, F., Pescalli, A., Oganessian, G., et al. 2017, *A&A*, 598, A23
 Nava, L., Vianello, G., Omodei, N., et al. 2014, *MNRAS*, 443, 3578
 Paczyński, B. 1998, *The Astrophysical Journal Letters*, 494, L45
 Pisani, G. B., Ruffini, R., Aimuratov, Y., et al. 2016, *ApJ*, 833, 159
 Rueda, J. A., & Ruffini, R. 2012, *ApJ*, 758, L7
 Ruffini, R., Bianco, C. L., Frascchetti, F., Xue, S.-S., & Chardonnet, P. 2001c, *ApJ*, 555, L117

- Ruffini, R., Salmonson, J. D., Wilson, J. R., & Xue, S.-S. 1999, *Astronomy and Astrophysics Supplement*, 138, 511
- Ruffini, R., Wang, Y., Enderli, M., et al. 2015a, *ApJ*, 798, 10
- Ruffini, R., Muccino, M., Kovacevic, M., et al. 2015b, *ApJ*, 808, 190
- Ruffini, R., Muccino, M., Aimuratov, Y., et al. 2016a, *ApJ*, 831, 178
- Ruffini, R., Rueda, J. A., Muccino, M., et al. 2016b, *ApJ*, 832, 136
- Ruffini, R., Rodriguez, J., Muccino, M., et al. 2016c, [arXiv:1602.03545](https://arxiv.org/abs/1602.03545)
- Ruffini, R., Aimuratov, Y., Becerra, L., et al. 2017, *ArXiv e-prints*
- Ruffini, R., Wang, Y., Aimuratov, Y., et al. 2018a, *ApJ*, 852, 53
- Ruffini, R., Muccino, M., Aimuratov, Y., et al. 2018b, *ArXiv e-prints*
- Smartt, S. J. 2009, *ARA&A*, 47, 63
- Woosley, S. E. 1993, *ApJ*, 405, 273
- Woosley, S. E., & Bloom, J. S. 2006, *ARA&A*, 44, 507